PHYSICAL REVIEW B VOLUME 34, NUMBER 3 1 AUGUST 1986

Double electron-muon resonance of anomalous muonium in silicon

K. W. Blazey
IBM Zurich Research Laboratory, CH-8803 Rüschlikon, Switzerland

T. L. Estle and S. L. Rudaz
Physics Department, Rice University, Houston, Texas 77251

E. Holzschuh, W. Kündig, and B. D. Patterson
Physik Institut, Universität Zürich, 8001 Zurich, Switzerland
(Received 11 February 1986)

Double electron-muon resonance (DEMUR) is reported on anomalous muonium centers in silicon. Resonance of EPR transitions otherwise non-observable is detected by characteristic structure in the muon-spin-rotation (μSR) spectra. In order to explain the nature of this structure, the theory of DEMUR is extended to include inhomogeneous broadening of the EPR and μSR transitions owing to nuclear hyperfine interactions with the ^{29}Si nuclei present. The principal effect of this extension is that only one of the two μSR lines is split rather than both as predicted when nuclear hyperfine effects are neglected.

I. INTRODUCTION

When a positive muon is stopped in silicon, three types of defect centers may be generated.[1] In two types of these centers, the μ^+ interacts with an unpaired electron, forming paramagnetic centers analogous to muonium. The third type of defect is a μ^+ in a diamagnetic environment. The two types of muoniumlike defects have widely differing μ^+ hyperfine interactions. Normal muonium, Mu, has an isotropic hyperfine interaction which is significantly less than the free muonium value; it is 45% of the vacuum value for Si. Anomalous muonium, Mu*, has a very anisotropic hyperfine interaction with a $\langle 111 \rangle$ symmetry axis, whose average value is much smaller than for normal muonium, 1.5% of the vacuum value for Si. Anomalous muonium is particularly interesting in that there is no known hydrogen center even remotely resembling it. Indeed, no paramagnetic hydrogen centers have been observed in any semiconductor.

Anomalous muonium in both Si and Ge has an appreciable nuclear hyperfine interaction with nearby host nuclei with spin. This is evident by the increased depolarization rate or muon-spin-rotation (μSR) linewidth at low magnetic fields, below about 50 G for Si and about 500 G for Ge.[2] In the Paschen-Back regime of large magnetic fields the muon spin and the nuclear spins are decoupled and there is no nuclear hyperfine broadening of the μSR lines.[3] This is particularly evident in measurements on the III-V compound crystals, GaAs and GaP, where fields of the order of 5 kG are required to obtain narrow lines.[4]

These muonium centers are studied by the muon spin-rotation (μSR) technique, essentially a free-precession magnetic-resonance method of studying the muon spin. Recently, it has been shown that muoniumlike centers may be investigated with a double-electron muon-resonance[5] (DEMUR) technique if an rf field is applied perpendicular to the static magnetic field. Coherence phenomena are observed when the intense rf magnetic field is tuned on or near resonance with one of the transitions of the muoniumlike center. Characteristic splittings of the μSR lines were first observed in quartz when the rf field drove one of the intratriplet μSR transitions. Here, we investigate the effect of the rf field tuned near resonance with one of the EPR transitions of the anomalous muonium center in silicon. These EPR transitions have extremely weak amplitudes in the normal μSR spectrum, and are therefore not observable by means other than the DEMUR experiment described here.

Observation of the EPR transitions of Mu* would provide a direct way of measuring the electronic g factor. However, the inhomogeneous linewidths of the EPR transitions were so large for Mu* in Si, that accurate values of the g factor could not be obtained, as will be explained. The unusual spectra observed can be understood in terms of a reasonably large nuclear hyperfine interaction as the source of the inhomogeneous broadening.

In the next section, DEMUR of anomalous muonium in silicon in the absence of nuclear hyperfine interaction with nearby ^{29}Si nuclei will be described. Following that, the effect of nuclear hyperfine interaction will be introduced. After a description of the experiment and results, the theory will then be compared with the observations.

II. THEORY

A. Anomalous muonium without nuclear hyperfine interaction: transitions and DEMUR

When nuclear hyperfine interaction is ignored, then the spin Hamiltonian for Mu* is

$$\mathscr{H}=g_{\parallel}\mu_B H_z S_z + g_{\perp}\mu_B (H_x S_x + H_y S_y) + A_{\parallel} S_s I_z + A_{\perp}(S_x I_x + S_y I_y) - g_\mu \mu_\mu \mathbf{H}\cdot\mathbf{I}\ , \qquad (1)$$

where z is the particular $\langle 111 \rangle$ axis which is the symmetry axis of the Mu* under consideration. Both the electronic spin S and muon spin I are $\frac{1}{2}$. Solving the eigenvalue problem for this Hamiltonian in the case that **H** is perpendicular to z, gives the energy-level diagram in Fig. 1. The transitions which are strongly allowed magnetic dipole transitions for the muon and for the electron above about 40 G are shown.

In the DEMUR experiment described in this paper, one of the two EPR transitions is driven by a large rf field, and the resultant structure in the two μSR lines is sought. The first DEMUR experiment was performed on normal muonium in quartz,[5] where it was shown that if both levels of the μSR transition are also those of the driven EPR transition, a triplet will be observed in the μSR spectrum. If only one level of the μSR transition is involved in the driven EPR transition, then a doublet will be observed in the μSR spectrum. This latter case clearly applies here to Mu*. It was also shown earlier[5] that the frequencies of the two components arising from the splitting of a single μSR line are

$$\nu=\nu_\mu \mp S_e \tfrac{1}{2}\{[(\nu_{\rm rf}-\nu_e)^2+\nu_R^2]^{1/2}\mp(\nu_{\rm rf}-\nu_e)\} , \qquad (2)$$

and the corresponding amplitudes of these two components are

$$a=\tfrac{1}{2}a_\mu\left[1\pm\frac{\nu_{\rm rf}-\nu_e}{[(\nu_{\rm rf}-\nu_e)^2+\nu_R^2]^{1/2}}\right] . \qquad (3)$$

In these equations, ν_μ and a_μ are the frequency and amplitude of the μSR line with no rf field applied, ν_e is the frequency of the driven EPR line, $\nu_R=\frac{1}{2}g\mu_B H_1$ is the Rabi frequency for the properly rotating component of $\mathbf{H}_1$, and $S_e=\pm1$ for the higher- (lower-) frequency EPR line. The field $\mathbf{H}_1$ is the amplitude of the oscillating rf field perpendicular to the static field in this experiment. It is not perpendicular to the Mu* symmetry axis which however is orthogonal to the static magnetic field. The g factor is the standard value appropriate to the direction of $\mathbf{H}_1$.

The prediction of this theory is that both the μSR lines will be split equally, the resulting amplitudes of the two lines that result from each will be equal on resonance, and that on resonance the splittings will be proportional to H_1 but there will be nothing else which depends on H_1. As we shall show, the observations are inconsistent with this theory which was successful in explaining DEMUR in quartz. The reason is that nuclear hyperfine interactions are not important in quartz and have been neglected until now.

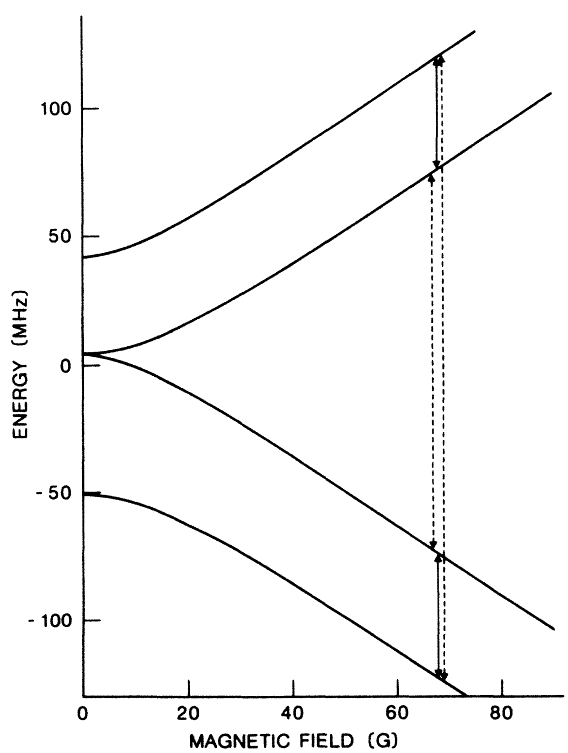

FIG. 1. Energy-level diagram of Mu* in silicon with $\mathbf{H}\perp\hat{\mathbf{z}}$. The Mu* hyperfine-interaction parameters are $A_{\parallel}=16.8$ MHz and $A_{\perp}=92.6$ MHz. The μSR transitions are shown by solid lines and the EPR transitions by dashed lines.

B. Anomalous muonium with nuclear hyperfine interactions: energies, transitions, and qualitative description of DEMUR

The only stable isotope of silicon with a nonzero nuclear spin is ^{29}Si whose spin is $\frac{1}{2}$ and whose natural abundance is 4.7%. Consequently, we need to consider primarily the problem of DEMUR in the presence of nuclear hyperfine interaction with a single nucleus of spin $\frac{1}{2}$. When, further, we make the reasonable approximation that this nuclear hyperfine interaction is isotropic, then the energy-level diagram of Fig. 2 results. Each of the EPR and μSR transitions is now split into two, but as the magnetic field increases the splitting of the μSR lines decreases and that of the EPR lines *increases*.

The interpretation of the field dependence of the μSR linewidth of Mu* in Ge implies that there are appreciable but different nuclear hyperfine interactions from ^{73}Ge nuclei at several different sites.[2] Our study of the linewidths for Mu* in Si reported here also supports this view. Therefore, the μSR and EPR lines are inhomogeneously broadened with widths resulting from a distribution of the nuclear hyperfine splittings shown in Fig. 2.

A qualitative understanding of the present experiment can be deduced from a simple perturbation treatment of Mu* for an isotropic nuclear hyperfine interaction with a single nucleus of spin $\frac{1}{2}$. Because of the low fields used, the nuclear and muon Zeeman interaction will be neglected. Taking the applied magnetic field perpendicular to the Mu* symmetry axis, as in the experiment, and considering only the limiting case that $g_\perp\mu_B H \gg |A_\perp|+|A_\parallel|$ and $g_\perp\mu_B H \gg |A|$, where A is the isotropic nuclear hyperfine parameter, the energies of the eight states are given approximately by

$$E=M_S g_\perp\mu_B H(1+\epsilon_S)+M_S M_I A_\perp+M_S M_n A(1-\epsilon_S) , \qquad (4)$$

where

$$\epsilon_S=\frac{1}{8}\left[\frac{A_\perp-4M_S M_I A_\parallel}{g_\perp\mu_B H}\right]^2 .$$

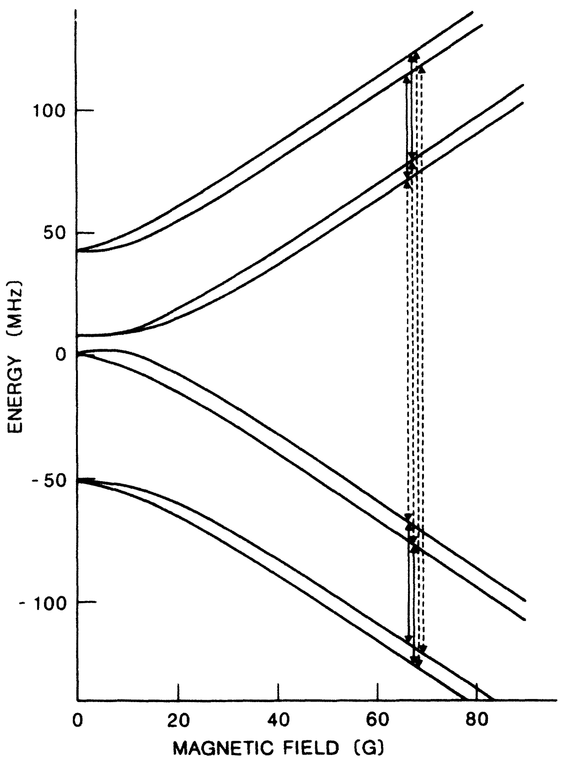

FIG. 2. Energy-level diagram of Mu* in silicon interacting with a single ^{29}Si nucleus with an isotropic hyperfine-interaction constant of 15 MHz. The μSR transitions are shown by solid lines, and the EPR transitions by dashed lines.

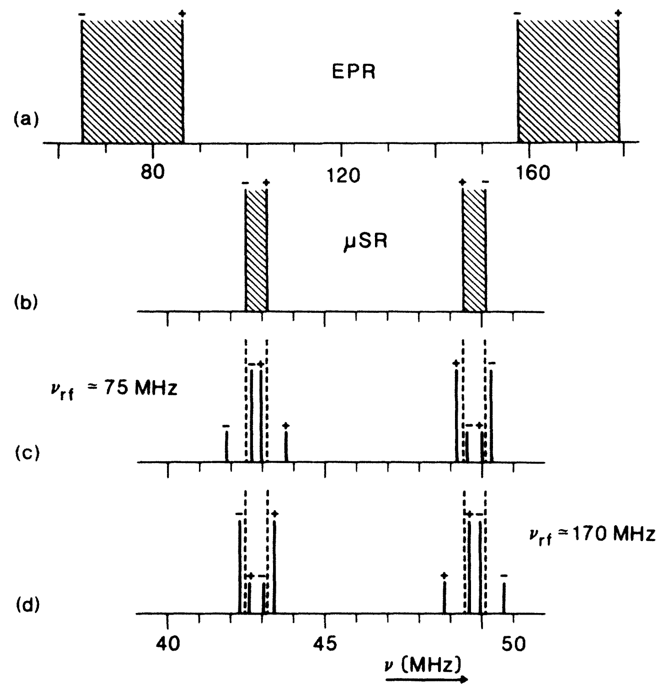

FIG. 3. Inhomogeneous broadening of (a) EPR and (b) μSR lines by hyperfine interaction with a single ^{29}Si nucleus at various possible neighboring sites. The crosshatched area corresponds to the distribution of hyperfine interactions. The effect of this inhomogeneous broadening on the μSR lines is illustrated while driving the center of (c) the low-frequency EPR line and (d) the high-frequency EPR line in the case of an isotropic nuclear hyperfine interaction of 23 MHz and an applied magnetic field of 40 G.

The quantities M_S, M_I, and M_n are the electronic, muonic, and nuclear azimuthal quantum numbers, respectively.

For a field greater than about 40 G, these results correspond to those of Fig. 2, especially in having all of the correct relative positions of levels and transitions. The frequencies of the two allowed EPR transitions are given by

$$h\nu_{\pm}^{(e)}=g_{\perp}\mu_B H(1+\eta)\pm\tfrac{1}{2}A_{\perp}+M_n A(1-\eta)\ , \tag{5}$$

where

$$\eta=\frac{1}{8}\frac{A_{\parallel}^2+A_{\perp}^2}{(g_{\perp}\mu_B H)^2}$$

and the two strong μSR transitions yield the μSR frequencies

$$h\nu_{\pm}^{(\mu)}=\tfrac{1}{2}\,|A_{\perp}|\left[1\pm\frac{1}{2}\frac{A_{\parallel}}{g_{\perp}\mu_B H}\left[1-M_n\frac{A}{g_{\perp}\mu_B H}\right]\right]. \tag{6}$$

The spectra resulting from these equations are shown in Figs. 3(a) and 3(b). The values of the parameters used in the figures are not those of this experiment; the field is lower and the nuclear hyperfine parameter is larger than for the experiment. In addition, Eqs. (4)—(6) are not very accurate for these values. Nonetheless, Figs. 3(a) and 3(b) have all the correct qualitative features and are easier to illustrate than on a figure with more realistic parameters. In Figs. 3(a) and 3(b), the solid vertical lines correspond to the frequencies of the transitions for a specific value of the nuclear hyperfine parameter. The sign of AM_n is shown for each of these lines. In a silicon crystal, the value of A will depend on the site occupied by the ^{29}Si. This causes a distribution of A values yielding inhomogeneously broadened lines made up of a number of spin packets with different A values as represented by the crosshatched regions in Figs. 3(a) and 3(b). Note that the μSR lines are considerably narrower than the EPR lines. In addition, the spin packets with positive AM_n are on the high-frequency side of both EPR lines and of the lower-frequency μSR line but on the low-frequency side of the higher-frequency μSR line. These results are independent of the signs of $A_{\parallel}$, $A_{\perp}$ and A.

A qualitative understanding of DEMUR on Mu* results from knowing what happens to the spin packets for a specific value of A when the rf corresponds to the center of one of the two EPR lines. To do this, we use the results of Estle and Vanderwater[5] for normal muonium in quartz applied to the two cases shown in Fig. 4, i.e., Eqs. (2) and (3) of this paper. For example, if the rf is just below the resonant value of the low-frequency EPR line then both μSR lines will split into two. The stronger component is below the μSR frequency without rf and displaced less than the weaker, higher-frequency component of the doublet in each case. Figure 4 shows the

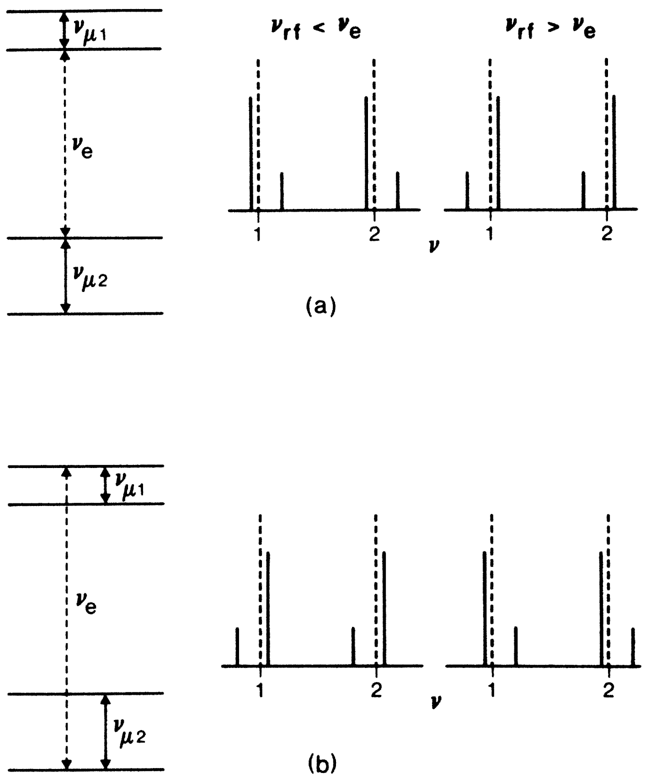

FIG. 4. Splitting of the two Mu* 90° μSR lines when driving (a) the low-frequency and (b) the high-frequency EPR transitions slightly off resonance.

four qualitatively different possibilities of driving above or below each of the EPR transitions.

To apply this to Mu* in Si with inhomogeneous broadening of both the EPR and the μSR lines, consider what happens successively to the nuclear hyperfine lines with AM_n positive and negative when the rf is at the midpoint of the resultant inhomogeneously broadened line. Figures 3(c) and 3(d) show what happens for the two possible cases, driving the low- and high-frequency EPR lines, respectively.

If we consider driving the center of the low-frequency EPR line, we see from Fig. 3(a) that ν_{rf} will be below the line with $\mathrm{AM}_n > 0$. Thus, we apply the qualitative features of the left side of Fig. 4(a). The stronger member of the resultant doublet is on the low-frequency side which is closer to the center of the inhomogeneously broadened μSR line at the lower frequency but away from the center of the higher-frequency μSR line. The results for $AM_n < 0$ and for the high-frequency EPR line follow similarly and are shown in Figs. 3(c) and 3(d). If we mentally distribute the values of A, then we shall find a tendency to produce a splitting only if the stronger lines in the doublet are moved away from the center. Consequently, we can argue that if the low-frequency EPR line is driven, the high-frequency μSR line will split but not the low-frequency μSR line. The reverse will be true if the high-frequency EPR line is driven. These conclusions are consistent with the quantitative description of the next section and our observations.

C. Theory of DEMUR with nuclear hyperfine effects: quantitative description

In this section, we present a quantitative version of the theory of Secs. II A and II B. Both the EPR and μSR lines are assumed to be inhomogeneously broadened because of unresolved nuclear hyperfine structure. For simplicity, and because it is usually a reasonable approximation, we take the shape of the inhomogeneously broadened EPR line to be Gaussian. We also use the result valid for hyperfine structure with a single nuclear spin to argue that the displacement of a spin packet in the EPR line is proportional to the displacement of the corresponding spin packet in the μSR line [see for example, the lines marked + in Figs. 3(a) and 3(b)]. Thus, in the absence of rf, the μSR lines also have a Gaussian shape. The effect of driving a particular spin packet in the EPR line but being off resonance in general is described by Eqs. (2) and (3) [see also Figs. 3(c), 3(d), and 4]. Integrating this over the inhomogeneous Gaussian line shapes yields the normalized line shape, $A(\nu)$, for the effects of an rf field

$$A(\nu)=\frac{1}{2\sqrt{2\pi}\sigma_\mu}\sum_{i=1}^{2}\exp\left[-\frac{1}{2\sigma_e^2}(\nu_i+\nu_{\mathrm{rf}}-\nu_e)^2\right]\frac{1+\frac{1}{2}S_e\dfrac{\nu_i}{\nu_d-\eta\nu_i}}{\left|1+S_\mu S_e\dfrac{\sigma_e}{2\sigma_\mu}\left[1-\frac{1}{2}S_e\dfrac{\nu_i}{\nu_d-\eta\nu_i}\right]\right|}, \tag{7}$$

where

$$\nu_i=\frac{1}{\eta^2-\frac{1}{4}}\left[\eta\nu_d+\frac{(-1)^i}{2}[\nu_d^2+(\eta^2-\tfrac{1}{4})\nu_R^2]^{1/2}\right],$$

$$\nu_d=\nu-\nu_\mu+S_\mu\frac{\sigma_\mu}{\sigma_e}(\nu_{\mathrm{rf}}-\nu_e),$$

$$\eta=-\tfrac{1}{2}\left[S_e+2S_\mu\frac{\sigma_\mu}{\sigma_e}\right].$$

The values σ_μ and σ_e are proportional to the widths without rf of the μSR and EPR lines, respectively (the full width at half amplitude is $2\sqrt{2\ln 2}\sigma$). The signs S_μ and S_e are $+1$ or -1 depending on whether the high- or low-frequency lines are considered (μ for μSR line, e for EPR line). The center of the inhomogeneous EPR line is ν_e, and the center of the μSR line is ν_μ. The radio frequency is ν_{rf}, and ν_R is the Rabi frequency, about $1.4H_1$ MHz if the amplitude of the oscillating field, H_1, is in G.

This spectrum has singularities for one of the two μSR lines as shown in Fig. 5. In particular, if $S_\mu S_e = -1$, then for a range of frequencies $A(\nu)=0$. Integrable singularities flank the region in which $A(\nu)=0$ and occur at

$$\nu=\nu_\mu - S_\mu \frac{\sigma_\mu}{\sigma_e}(\nu_{\rm rf}-\nu_e) \pm \left[\frac{\sigma_\mu}{\sigma_e}\left[1-\frac{\sigma_\mu}{\sigma_e}\right]\right]^{1/2} \nu_R \; . \qquad (8)$$

If $S_\mu S_e = +1$, then $A(\nu) \neq 0$ for all finite values of ν.

Examples of both cases are contained in Fig. 5. To better describe the Fourier transforms of the experimentally obtained time-differential muon polarization, the line shape in Eq. (7) has been convoluted with a Gaussian function. The integral under $A(\nu)$ in the region of the singularities is relatively large as long as $\nu_R \lesssim \sigma_e$. However, for $\nu_R > \sigma_e$ the singularities become unimportant in the convoluted line shape. They are replaced, in a sense, by the fact that $A(\nu)$ has two peaks when $\nu_R > \sigma_e$ (at least when $\nu_{\rm rf} = \nu_e$). These peaks occur near $\nu = \nu_\mu \pm \frac{1}{2}\nu_R$ on resonance [see Fig. 5].

The other line in the μSR spectrum will have $S_e S_\mu = +1$. It has a single peak at $\nu = \nu_\mu$ except for $\nu_R > \sigma_e$ when two peaks also occur. These peaks are not separated by quite as much for the line with $S_e S_\mu = -1$. This is also shown in the plots of $A(\nu)$ in Fig. 5.

In all cases observed in this experiment, there was only a splitting of the μSR line corresponding to $S_e S_\mu = -1$; that is, when the high-frequency (low-field) EPR line is driven ($S_e = 1$) then only the low-frequency μSR line is split ($S_\mu = -1$), but when the low-frequency (high-field) EPR line is driven ($S_e = -1$) then only the high-frequency μSR line is split ($S_\mu = 1$). Thus, we can immediately conclude that we are dealing with the case $\nu_R \leq \nu_e$.

Convolution of the line shape of Eq. (7) with a Gaussian function is intended to allow for broadening mechanisms other than nuclear hyperfine effects but primarily for the effect of the discrete Fourier transform used to display the frequency spectrum. Using values of the parameters in the theory comparable to those considered to be approximately correct, we find on resonance the spectrum of Fig. 6(a).

In addition to the splitting of just one line, the calculations give several other qualitative features of the observed data. If ν_R, or its equivalent, the amplitude of the rf magnetic field, is increased, then the peak amplitude of the spectra will decrease as roughly $1/H_1$. If the radio frequency is moved from the center of the inhomogeneously broadened EPR line, then one of the two components of the split line observed on resonance will decrease, whereas the other will increase. Several of these features are illustrated in Fig. 6. In addition, the splitting of the μSR lines on resonance is calculated to be less, often much less, than the Rabi frequency, which would be the splitting in the μSR lines if $\nu_R > \sigma_e$. The qualitative features of these calculations agree with the observations as discussed in the last section.

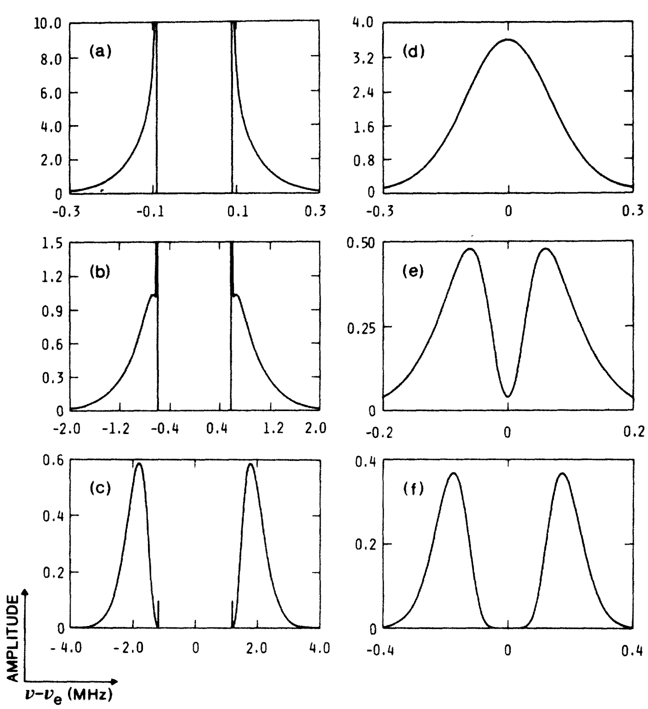

FIG. 5. DEMUR amplitude line shapes calculated from Eq. (7) on resonance ($\nu_{\rm rf} = \nu_e$). The left column is for $S_\mu S_e = -1$, the line which is split by the rf field. The right column is for $S_\mu S_e = +1$, the line which is not split in this experiment. The parameters employed were $\sigma_\mu = 0.1$ MHz and $\sigma_e = 1.0$ MHz. (a) and (d) used $\nu_R = 0.3$ MHz, (b) and (e) $\nu_R = 2.0$ MHz, and (c) and (f) $\nu_R = 4.0$ MHz. Note the different scales both for amplitude and for frequency ($\nu - \nu_e$).

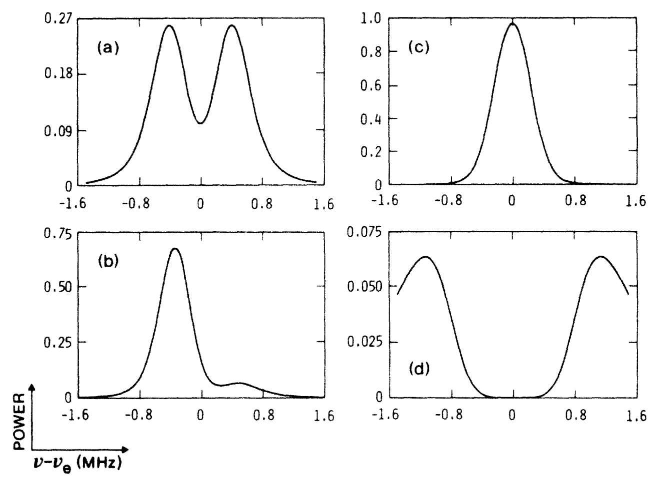

FIG. 6. DEMUR power line shapes for $S_\mu S_e = -1$ calculated by convoluting a Gaussian function with $A(\nu)$ from Eq. (7). (a) was calculated using parameters which gave reasonable agreement with experiment (see Figs. 7 and 8). These were $\sigma_\mu = 0.03$ MHz, $\sigma_e = 5.0$ MHz, and $\sigma_G = 0.23$ MHz, where σ_G is for the Gaussian, for all the figures. (a) and (b) used $\nu_R = 2.67$ MHz, i.e., $H_1 = 1.91$ G, (c) $\nu_R = 1.34$ MHz, and (d) $\nu_R = 5.34$ MHz. (a), (c) and (d) were calculated on resonance, $\nu_{\rm rf} = \nu_e$, while (b) used $\nu_{\rm rf} - \nu_e = 2.8$ MHz, i.e., 1 G below resonance. Note the different power scales for the different figures.

III. EXPERIMENT AND RESULTS

The experiments were performed at the muon facility of the Swiss Institute for Nuclear Research. A high-purity silicon crystal with $\rho = 30,000\ \Omega\,\mathrm{cm}$ and 5×10^{11} active carriers per cm^3 at room temperature obtained from Topsil was measured at both 77 and 4.2 K. A bath cryostat was used with a tuned coupled transformer immersed in the liquid nitrogen. The Si crystal could be mounted either directly in the liquid nitrogen or in a helium Dewar inserted in the tuned coupled transformer. This transformer had a two-turn copper-wire primary coil separated ~ 10 mm from a three-turn secondary coil. A high-voltage variable capacitor in the secondary allowed tuning up to approximately 210 MHz. Another capacitor in the primary coil allowed a 50-Ω matching to the source which was an HP 8640B signal generator driving an ENI 550L 50-W broadband amplifier. The transformer produced a rf field orthogonal to the incoming muon beam and the static field of an air core electromagnet. The circuit Q was approximately 100, and the rf field was monitored with a single-loop pickup coil at the secondary. This arrangement produced fields up to about 3-G amplitude.

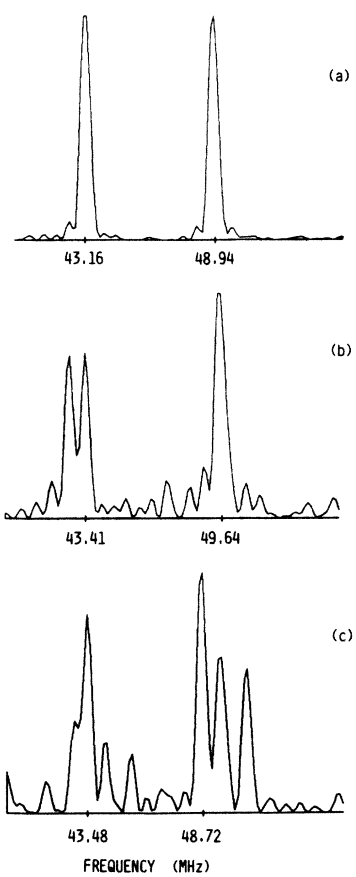

FIG. 7. DEMUR of Mu* in silicon at 4.2 K. (a) The two Mu* 90° μSR lines with no rf field. (b) 50-G static magnetic field and 196-MHz rf field driving the high-frequency EPR transition produces a splitting only of the low-frequency μSR line. (c) 85-G static magnetic field and 196-MHz rf field driving the low-frequency EPR transition produces a splitting only of the high-frequency μSR line. The high-frequency line, at about 50.6 MHz, is not part of the spectrum but rather the cyclotron frequency.

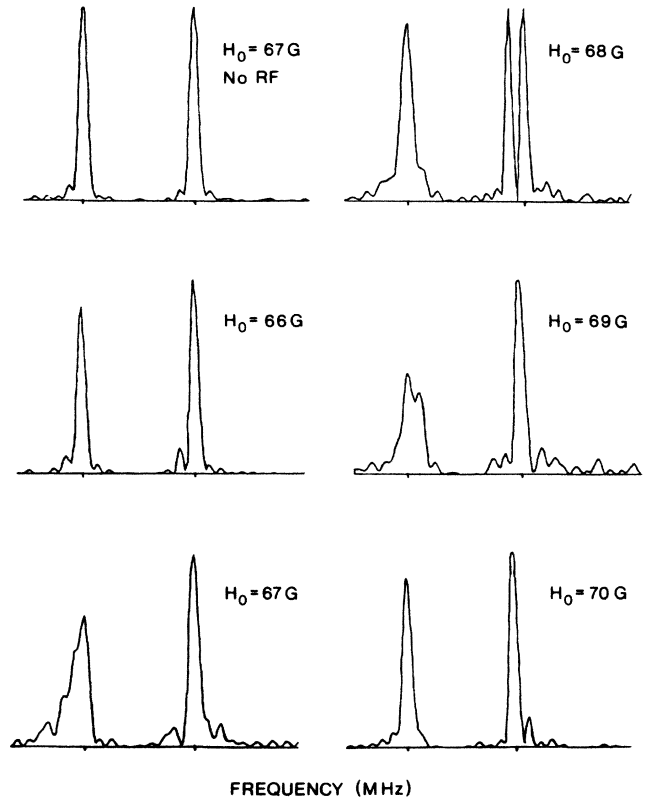

FIG. 8. DEMUR of Mu* in silicon at 77 K showing the effect of moving through the resonance of the low-frequency EPR transition. For the 150-MHz rf field, resonance occurs with a 68-G static magnetic field.

Time-differential transverse-field muon-spin-rotation events were collected in two histograms from which the precession frequencies, amplitudes, and relaxation rates were determined by multifrequency fits. A trial experiment with a quartz crystal warmed to near room temperature by blowing heated air over it showed that with 5 W into the transformer, the low-frequency intratriplet μSR transitions were split by 2.6 MHz. The rf was set at 181.5 MHz, the frequency of the high-frequency intratriplet μSR transition. The pickup voltage for higher input powers was not stable over the period of hours required for each measurement. It was found necessary to readjust the input to the power amplifier to maintain a pickup voltage constant to within 5% even for powers of the order of 5 W.

DEMUR effects were sought for Mu* centers in Si whose principal axes were perpendicular to the static applied magnetic field. With a rf of 196 MHz, the low-and high-frequency EPR transitions were driven in a static field of 85 and 50 G, respectively, at 4.2 K. These conditions produced a splitting of the higher-frequency μSR line in the former case, and a splitting of the lower-frequency μSR line in the latter case. This is illustrated in Fig. 7, and confirms qualitatively the model of Sec II.

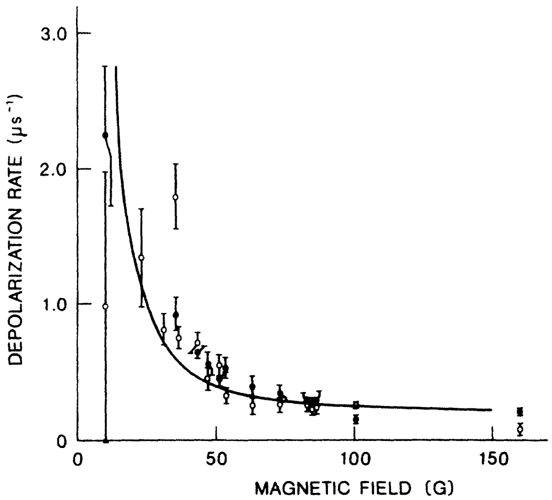

FIG. 9. Magnetic-field variation of the depolarization rate of the Mu* μSR transitions in Si. Low-frequency line (open circles); high-frequency line (solid circles). The solid curve is a least-squares fit to $\lambda=\lambda_\infty+C/H^2$.

Further experiments were performed at 77 K with 150-MHz rf. No difference could be detected in the results other than the known shift of the μSR lines with temperature and field. In this case, the low-frequency EPR transition was driven, and the high-frequency μSR transition split or even broadened so much in the largest rf field available that it was no longer observable. The results with a moderate rf field are shown in Fig. 8. The resonance condition is obtained with a 68-G static magnetic field. If the static field is adjusted 1 G off resonance in either direction, then the splitting will disappear. In addition, the line which was not split on resonance is broadened. This also disappears on adjusting the static field another 1 G further off resonance in either direction.

In addition to the DEMUR results summarized above, we made measurements with no rf field applied for comparison. These data and measurements at a few other static fields allow us to plot the depolarization rate for Mu* in Si versus magnetic field, much as has been done in the past[2] for Mu* in Ge. These data are shown in Fig. 9. The data of Fig. 9 can be described approximately by $\lambda=\lambda_\infty+C/H^2$. The term proportional to H^{-2} arises from unresolved nuclear hyperfine structure in the high-field limit, but it should not accurately describe λ at fields below about 50 G. Fitting all of our data, we obtain $\lambda_\infty=0.200\pm0.012\mu\text{sec}^{-1}$ and $C=494\pm34$ $G^2\mu\text{sec}^{-1}$ with $\chi_\nu^2=5.80$ and 33 degrees of freedom, i.e., a poor fit. The solid line in Fig. 9 is this fitted curve.

IV. DISCUSSION AND CONCLUSION

Figures 7 and 8 summarize most of the features observed. The most noticeable feature is the failure to see a splitting of both μSR lines. Rather, when the rf magnetic field is on resonance with the high-field (low-frequency) EPR line, the high-frequency μSR line splits but the low-frequency one does not. Driving the low-field (high-frequency) EPR line causes the low-frequency μSR line to split but not the high-frequency one. These results evolve consistently from our theoretical analysis is Subs. II B and II C. Fundamentally, it comes about because of the relationships of corresponding spin packets in the inhomogeneously broadened lines, as shown in Figs. 3(a) and 3(b). Whereas the spin packets are on the same sides of both EPR lines and the low-frequency μSR line the high-frequency μSR line is the opposite. Thus, the two μSR lines behave differently. The differences in driving the two EPR lines comes about because of the consequences of the theory of DEMUR (Ref. 5) applied to these two cases (see Fig. 4).

The largest splitting observed for any μSR line of Mu* arising from the rf field was about 0.8 MHz. This was considerably lower than the 2.6 MHz measured for quartz in the same apparatus, although at different temperatures. The Rabi frequency for Mu* should actually be larger by $\sqrt{2}$ than that in quartz. Thus, the splitting observed for Mu* in Si is about 4.6 times smaller than would have been expected on the basis of the quartz observation and the relative Rabi frequencies. The theoretical model presented in Sec. II C predicts that the splitting observed may be considerably less than the Rabi frequency. As the rf field is increased, and thus also the Rabi frequency, the splitting becomes a larger fraction of the Rabi frequency but the peak amplitudes in the power spectra decrease, varying as about $1/H_1^2$. For Rabi frequencies much lower than that required to give a splitting of 0.8 MHz, there is no splitting at all. Thus, the splitting observed seems to be just above the threshold for splittings, and large splittings are not observed because of the fact that our Fourier power spectra are very weak even though we collected a large number of good events ($\sim$50 000 000 typically).

The loss of the splitting as the static field is changed from the resonant value results from the theoretical model of Sec. II C because the effects of being off resonance are to increase one of the two components of the split line and decrease the other. Owing to the poor quality of our power spectra, the weaker line is not observed.

The EPR linewidth could not be determined from the experimental results because H_1, could not be reliably measured independently. Thus, we could obtain good agreement with our observations for a range of EPR linewidths of at least a factor of 10 by allowing for a reasonable range of possible H_1 values, a factor of 3. However an independent estimate of the EPR linewidth could be obtained from the measured depolarization rate versus static field of Fig. 9. Using a perturbation treatment of the nuclear hyperfine effects to convert this to an EPR linewidth gives values close to 12 MHz for the full width at half maximum of the EPR line ($\sigma_e=5$ MHz) which was used in the calculations.

Because of the width of the EPR lines and the relatively low radio frequency used, the location of the EPR lines could only be determined to about 1%. To this accuracy, the electronic g factor is 2.00, a result consistent with earlier reports using different approaches.[6]

The DEMUR spectrum of Mu* in Si has been measured by driving EPR transitions which are nonobservable otherwise. The spectrum differed markedly from that previously observed for normal muonium in quartz. All of the observable features of the DEMUR of Mu* in silicon can be explained by including nuclear hyperfine interactions in the theory of DEMUR. These nuclear hyperfine interactions cause about a 12-MHz EPR linewidth as reflected in the field dependence of the μSR linewidth without an external rf field, and is consistent with the DEMUR results.

ACKNOWLEDGMENTS

We should like to acknowledge stimulating discussions with H. Keller and W. Baechtold, and the assistance of D. P. Spencer on Figs. 5 and 6. The technical assistance of H. P. Ott and H. Nievergelt is gratefully acknowledged. This work was supported by the National Science Foundation under Grant No. DMR-79-09223.

[1]B. D. Patterson, A. Hintermann, W. Kündig, P. F. Meier, F. Waldner, H. Graf, E. Rechnagel, A. Weidinger, and T. Wichert, Phys. Rev. Lett. **40**, 1347 (1978).

[2]T. L. Estle, M. E. Warren, and B. D. Patterson, Hyperfine Interact. **17-19**, 589 (1984); T. L. Estle, S. L. Rudaz, E. Holzschuh, R. F. Kiefl, B. D. Patterson, W. Kündig, and K. W. Blazey, *ibid.* **17-19**, 623 (1984).

[3]R. F. Kiefl, E. Holzschuh, H. Keller, W. Kündig, P. F. Meier, B. D. Patterson, J. W. Schneider, K. W. Blazey, S. L. Rudaz, and A. B. Denison, Phys. Rev. Lett. **53**, 90 (1984).

[4]R. F. Kiefl, J. W. Schneider, H. Keller, W. Kündig, W. Odermatt, B. D. Patterson, K. W. Blazey, T. L. Estle, and S. L. Rudaz, Phys. Rev. B **32**, 530 (1985).

[5]T. L. Estle and D. A. Vanderwater, Phys. Rev. B **27**, 3962 (1983); J. A. Brown, R. H. Heffner, M. Leon, S. A. Dodds, T. L. Estle, and D. A. Vanderwater, *ibid.* **27**, 3980 (1983).

[6]B. D. Patterson, A. Hintermann, W. Kündig, P. F. Meier, F. Waldner, H. Graf, E. Recknagel, A. Weidinger, and T. Wichert, Phys. Rev. Lett. **40**, 1347 (1978); K. W. Blazey, T. L. Estle, E. Holzschuh, P. F. Meier, B. D. Patterson, and M. Richner, Phys. Rev. B **33**, 1546 (1986).